1636

Ecological Applications, 4(2), 1994, pp. 322–343

ECOLOGICAL REMOTE SENSING AT OTTER: SATELLITE MACROSCALE OBSERVATIONS[1]

SAMUEL N. GOWARD
Laboratory for Global Remote Sensing Studies, Department of Geography, University of Maryland, College Park, Maryland 20742 USA

RICHARD H. WARING
College of Forestry, Oregon State University, Corvallis, Oregon 97331 USA

DENNIS G. DYE AND JINGLI YANG
Laboratory for Global Remote Sensing Studies, Department of Geography, University of Maryland, College Park, Maryland 20742 USA

Abstract. Coarse, global-scale, satellite remotely sensed observations are compared with ground measurements collected during the OTTER study. The objective was derivation of ecological and environmental variables from the satellite data needed to define primary production in western Oregon. Observations from the TOMS sensor and the AVHRR sensor provide estimates of incident PAR radiation, intercepted PAR, atmospheric humidity, air temperature, vapor pressure deficit, and drought. The satellite observations compared favorably with the coincident ground measurements, but the strength of the relation was modest in some cases. Atmospheric attenuation of the remotely sensed measurements and ground measurement quality both limit stronger relations. This study demonstrates that satellite remote sensing is capable of providing information needed for macroscale ecological monitoring. Currently, it appears possible, from AVHRR and TOMS observations, to derive periodic approximations of ecological conditions sufficient to drive a simple-production-efficiency-type model. More refined remote-sensing methods will be needed to provide the type of measurement precision required by more refined ecosystem models.

Key words: accuracy of remote-sensing signals; air temperature; drought; humidity; incident PAR; intercepted PAR; interpretation of remote-sensing signals; Oregon transect; OTTER project; satellite remote sensing; vapor pressure deficit.

INTRODUCTION

One of the primary goals of the Oregon Transect Ecosystems Research (OTTER) study was to evaluate use of coarse, global-scale, satellite remotely sensed observations to characterize the ecological properties and environmental conditions observed across the Oregon transect. Previous research has suggested that satellite remote sensing provides measurements needed to evaluate global patterns of ecological processes (Justice et al. 1985, Tucker et al. 1985, 1986, Goward 1989, Heimann and Keeling 1989, Prince et al. 1990, Townshend et al. 1991). However, there have been few opportunities to directly compare coincident ground and satellite measurements. The OTTER study region provided a unique opportunity to carry out this comparison because across the OTTER environmental gradient we have observed a variation in spectral vegetation index measurements (e.g., normalized-difference vegetation index) that is equivalent to that observed across the entire North American continent (Goward et al. 1985).

This study contributes to our objective of defining methods to monitor biospheric productivity with satellite measurements alone. Previously, we discovered a strong correlation between the satellite normalized-difference vegetation index (NDVI) measurements and annual net primary production at continental and global scales (Goward and Dye 1987, Goward et al. 1987, Koomanoff 1989). We have also had some success in modeling this observed relation by using the NDVI measurements to estimate the fraction of photosynthetically active radiation (PAR) absorbed by vegetation canopies (Goward and Dye 1987). Ecological explanation of these results could lead to a simple model of biospheric activity that requires only satellite remote-sensing measurements to function. Such a model

[1] Manuscript received 16 February 1993; revised 15 August 1993; accepted 25 August 1993.

would provide an efficient means to study global patterns of biospheric productivity and would serve as an independent comparison to more detailed ecophysiological models of biological processes (Dickinson 1984, Sellers et al. 1986, Running and Coughlan 1988).

There is increasing evidence that the relation between satellite measurements and primary production occurs because of a direct relation between intercepted PAR and annual vegetation growth (Monteith 1977, Jarvis 1981, Landsberg 1986, Prince et al. 1990, Field 1991). This "production-efficiency-model" (PEM) approach may provide an effective means to study global-scale patterns of terrestrial photosynthetic activity from satellite remotely sensed observations. The OTTER study provided a significant opportunity to test this idea. Analysis of the OTTER field measurements found that primary production and intercepted PAR were well related, in western Oregon, only after the constraints of drought, high vapor-pressure deficits, and subfreezing temperatures are taken into account (Runyon et al. 1994 [this issue]). These results suggest that in order to monitor primary production with satellite observations, we will need to estimate not only incident PAR and intercepted PAR, but also the environmental constraints that limit use of intercepted PAR in photosynthesis. We had previously explored the potential for assessing land-surface environmental conditions with remote sensing (Goward et al. 1986, Goward and Hope 1989, Nemani et al. 1993), but the OTTER study provided the best opportunity to date to test these ideas.

Data and Methods

Results from the field measurements analysis (Runyon et al. 1994) indicated that in order to evaluate patterns of primary production across the Oregon transect we would need measurements of:

1) incident photosynthetically active radiation (PAR),
2) canopy interception of PAR,
3) air temperature,
4) vapor pressure deficit, and
5) drought related to soil moisture.

There is considerable evidence that remotely sensed observations may be used to extract such measurements (Asrar 1989, Goward 1989, Mooney and Hobbs 1990). However, there have been few studies that compare coincident satellite and ground measurements, particularly across such an environmental gradient. To remain within the context of our larger objective (i.e., global-scale analysis) we explore only satellite observations that provide frequent, global coverage.

Incident PAR from TOMS Observations

In this study we estimate incident PAR from longwave ultraviolet (UV; 0.37 μm) measurements collected by the Nimbus-7 TOMS (Total Ozone Mapping Spectrometer) sensor (Eck and Dye 1991, Dye 1992). It is also possible to estimate incident PAR from the AVHRR (advanced very high resolution radiometer) observations (Pinker and Laszlo 1992). At first glance the AVHRR approach would seem more appropriate because the AVHRR observes in the PAR wavelength region and it is the source of many other measurements. However, the AVHRR approach requires a priori knowledge of surface spectral reflectance in the 0.58–0.68 μm spectral region. For terrestrial surfaces this reflectance is highly variable in space and time (Bray 1966, Swain and Davis 1978, Stoner and Baumgardner 1981). In the ultraviolet region of the spectrum most land surfaces, with the exceptions of snow and salt flats, display reflectances between 2% and 5% (i.e., the earth is nearly a blackbody in the UV region). Since the atmospheric scattering that occurs in the UV is produced by the same atmospheric features that affect visible spectral wavelengths, it is possible to use the observed UV reflectance to estimate losses in the surface PAR flux without recourse to estimation of surface reflectance.

Validation was accomplished by comparison of the TOMS measurements with ground solar-irradiance observations collected at the five meteorological sites (Runyon et al. 1994 [this issue]). A LI-COR silicon photodiode pyranometer was employed at each of the meteorological observatories to measure incident solar radiation (LI-200SZ, LI-COR, Lincoln, Nebraska, USA). This sensor detects incident radiation in the 0.4–1.1 μm spectral range, which covers ≈80% of incident solar radiation (Kerr et al. 1967, Brest and Goward 1987). Hourly totals of incident radiation were recorded by automated data loggers at each station. Half the measured incident flux was assumed to be in PAR wavelengths (Monteith and Unsworth 1990).

TOMS observations

The TOMS sensor, deployed on the Nimbus-7 spacecraft, collects daily global measurements from a sun-synchronous polar orbit with an equatorial crossing time of 1200 (Eck et al. 1987). The instantaneous ground resolution of the TOMS sensor is 2500 km^2 at nadir, increasing to 30 000 km^2 at the largest off-nadir view angle.

An archive of observations from January 1979 to February 1990 has been compiled and processed by NASA (the National Aeronautics and Space Administration) as a part of their efforts to monitor the dynamics of atmospheric ozone. Within this program a global set of well-calibrated, geographically registered, monthly average TOMS UV measurements have been compiled from the original observations (Hwang et al. 1988). This was accomplished by navigating the observations with satellite ephemeris data and averaging, spatially and temporally, the observations within each cell of the output mapped-data array. The original PAR estimation study (Eck and Dye 1991) employed pro-

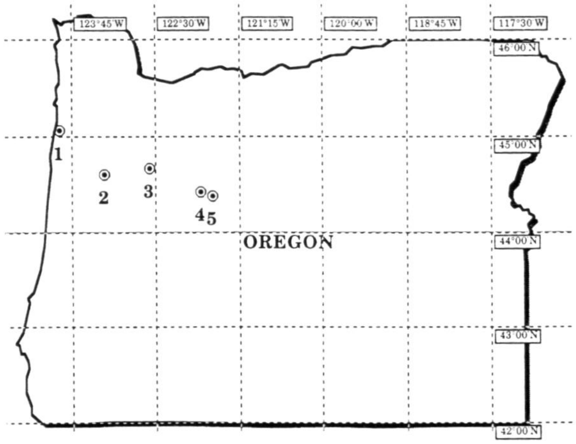

FIG. 1. Location map of OTTER sites in Oregon. The latitude–longitude grid represents the boundaries of the TOMS observation grid (1.25° latitude by 1° longitude). Note that sites 2 and 3 are contained in a single TOMS grid cell, as are sites 4 and 5.

cessed data arrays that had been compiled at a nominal ground resolution of ≈250 000 km^2 (4° latitude by 5° longitude). Dye (1992) recently completed a refined analysis of the same observations processed to a 50 000 km^2 (≈1° latitude by 1.25° longitude) spatial resolution. This latter data set was employed in this study.

Incident PAR

Employing a physical model of potential PAR irradiance for a cloudless atmosphere and the TOMS attenuation measurement, the mean monthly total incident PAR at the Earth's surface was computed at each TOMS grid cell (Eck and Dye 1991). Since atmospheric rather than surface conditions are estimated from the TOMS data, their relatively coarse spatial resolution, relative to the AVHRR 1.1-km^2 footprint, is not considered a problem. The atmosphere tends to be more homogeneous across regions than are typical landscapes. Also, the processed TOMS observations represent the monthly mean of atmospherically scattered radiation at noontime each day. We assumed that this monthly average noontime measurement is representative of monthly average atmospheric conditions during all daylight hours.

The OTTER meteorological observatories were installed between May and June 1989. Therefore, the comparison between the ground measurements and the TOMS PAR estimates was carried out for the period June 1989 to February 1990 (9 mo). The five OTTER meteorological stations are contained within three of the TOMS 1° grid cells (Fig. 1).

Intercepted PAR and environmental variables from AVHRR observations

The remainder of the desired variables were extracted from the advanced very high resolution radiometer (AVHRR) flown on the NOAA-11 polar-orbiting meteorological satellite. This sensor is a five-spectral-band scanning radiometer, with measurements in the visible (0.58–0.68 μm), the near-infrared (0.7–1.1 μm), and three wavelengths in the thermal infrared (3.5–3.9 μm, 10.3–11.3 μm and 11.5–12.5 μm) spectral bands. Details concerning its properties and operations can be found elsewhere (Schneider and McGinnis 1982, Kidwell 1988, Holben et al. 1990, Goward et al. 1991). The AVHRR observations used in the OTTER study were obtained from the EROS Data Center, Sioux Falls, South Dakota, USA.

EROS AVHRR data sets

In 1988 the EROS Data Center installed a reception antenna for AVHRR observations. This antenna permits acquisition of AVHRR observations for most of the coterminous United States. In 1989 EROS began production of biweekly composites of the western United States (Loveland et al. 1991, Eidenshenk 1992). We acquired the selected single-date observations from those used to produce the biweekly composites as well as selected additional observations between November and March. We procured observations from both 1989 and 1990, but concentrated on the 1990 observations in this analysis because more intensive ground studies were carried out during 1990.

The EROS Data Center carries out basic data processing, including navigation of the observations to a common map base and radiometric calibration. The map projection selected for the navigated images is the Albers Equal Area Projection with standard parallels at 29.5° N and 45.5° N, the central meridian at 96.0° W and the latitude of origin at 23.0° N. Navigation of the data includes use of NOAA-supplied satellite ephemeris data to geographically locate individual picture elements (pixels) and use of control points to remove residual registration error. This approach typically produces mapped observations with a registration precision of <1 km (one pixel).

The observations were radiometrically calibrated, with pre-flight NOAA measurements for the visible and near-infrared spectral bands and on-board calibration information for the thermal infrared channels, based on NOAA-defined procedures (Kidwell 1988). The original AVHRR observations were acquired at a digital precision of 10 bits, which produces an effective radiometric resolution of 0.1% in the reflective wavelengths and 0.1°C in the thermal infrared wavelengths. EROS employed the 10-bit precision in calculations but constrained the output files to 8 bits. In effect, this

TABLE 1. 1990 EROS AVHRR observations acquired for the OTTER study.

Day of year	Month	Day	Solar time	View zenith	View azimuth	Solar zenith	Selected
18	January	18	13:00:00	15°	119°	69°	*
20		20					
57	February	26					
58		27	13:04:00	40°	119°	56°	*
74	March	15					
80		21					
86		27					
89		30					
90		31	13:58:00	−24°	45°	49°	*
91	April	1					
92		2					
93		3					
95		5					
103		13					
120		30	13:12:00	11°	140°	34°	*
123	May	3					
129		9	13:16:00	8°	142°	32°	*
136		16					
158	June	7					
169		18	12:34:00	42°	139°	23°	*
175		24					
177		26					
194	July	13	13:08:00	19°	143°	27°	*
201		20					
204		23					
212		31					
215	August	3	12:27:00	44°	132°	28°	*
240		28					
247	September	4					
256		13	13:42:00	−11°	41°	48°	*
265		22					
272		29					
283	October	10					
284		11					
297		24	12:51:00	49°	131°	59°	*
310	November	6					
319		15	14:06:00	−15°	48°	70°	*
340	December	6					
355		21					
363		29	14:23:00	−32°	53°	76°	*

reduced the measurement precision of the resultant data files to 0.5% in the reflective bands and 0.5°C in the thermal bands.

Scene selection.—We selected the desired observations by visual inspection of microfiche imagery produced by the EROS Data Center. The criteria employed in image selections included (1) low cloud cover and (2) viewing zenith of <40° from nadir (the point on the Earth's surface directly below the satellite position) (Goward et al. 1991). In general we were able to acquire approximately four observations per month, but only after reducing the view angle constraint (Table 1). For this study we further selected the "best" scene acquired in each month for analysis. Best in this case was defined, first, relative to cloud cover and, second, relative to view zenith. This was done by inspection of the digital data, in image and plot form, on our computer image-processing system. We found that many of the apparently "cloud-free" scenes, as viewed in the microfiche, were still contaminated with clouds, which eliminated use of many of the acquired scenes.

Fraction of intercepted PAR from NDVI

We estimated fraction of canopy PAR interception (f_{IPAR}) from normalized-difference vegetation index (NDVI) measurements. The NDVI is computed as

$$\mathrm{NDVI} = \frac{\mathrm{NIR} - \mathrm{VIS}}{\mathrm{NIR} + \mathrm{VIS}}, \tag{1}$$

where VIS = visible wavelength measurement and NIR = near-infrared wavelength measurement. Previous research has indicated that, in general, there is a simple linear relation between fractional IPAR and NDVI (Kumar and Monteith 1982, Daughtry et al. 1983, Asrar et al. 1984, Sellers 1986, Choudhury 1987). We have further explored this relation and found that a single midday NDVI measurement is well related to fractional absorbed PAR (f_{APAR}), which occurs over a diurnal cycle as well as during periods with overcast skies (Goward and Huemmrich 1992). In the OTTER ground measurements only f_{IPAR} was measured (Runyon et al. 1994 [this issue]). Except when there is considerable senescent foliage in canopies, f_{IPAR} and f_{APAR} are well related (Asrar 1989).

Canopy f_{IPAR} tends to vary slowly, with changes in foliage magnitude and pigment absorption. Therefore once-per-month NDVI measurements were expected to provide an adequate assessment of seasonally varying f_{IPAR}. We computed the mean and standard deviation for a 3 × 3 array of observations, centered on the latitude and longitude of each OTTER study site, to characterize site f_{IPAR}. We employed this area average because (1) there is some residual uncertainty (±1 km) concerning the precise location of each observation, and (2) the standard deviation provides an internal estimate of the reliability of the measurements to characterize site conditions. We also extracted the mean and standard deviation of the visible and near-infrared measurements to provide further guidance concerning possible unique site properties and/or atmospheric conditions that might disrupt the assessment of surface conditions.

To evaluate the satellite f_{IPAR} estimates we used two separate measurements from the field studies: (1) the fractional intercepted PAR measurements collected during mid-growing season (Runyon et al. 1994) and (2) spectrometer measurements collected 500 m above the canopy from an ultralight aircraft (Peterson and Waring 1994). The former measurements provided an assessment of the validity of the satellite-inferred f_{IPAR} at mid-season. The ultralight-collected spectrometer observations provided a means to compare the NDVI observed near the ground with that from the satellite.

Environmental variables and TIR measurements

The environmental variables are estimated, in part, from the AVHRR thermal infrared (TIR) observations. Planck's law predicts, as a function of wavelength, an exponential relation between a material's kinetic temperature and its electromagnetic emissions (Wolfe 1965, Monteith and Unsworth 1990). Thus, remote-sensing TIR observations may serve as useful indicators of environmental conditions in ecosystems. The simple Planck predictions are disrupted in remotely sensed observations by atmospheric attenuation, particularly water vapor, and by material emissivity properties (Price 1989). These convolutions of the TIR signal require attention in analysis, but when adequately addressed may provide considerable additional information of value in ecological research.

Land surface temperatures.—The dual TIR spectral sensors on the AVHRR (channel 4, 10.3–11.3 μm, and channel 5, 11.5–12.5 μm) were designed to evaluate atmospheric water vapor attenuation in the 10–12 μm spectral region, with the objective of producing accurate ocean surface temperatures (Prabhakara et al. 1974, Deschamps and Phulpin 1980, McClain et al. 1985). In essence, the longer wavelength channel is attenuated more strongly by water vapor and therefore records lower radiometric temperatures than the shorter wavelength channel. This difference in radiometric temperatures between the two channels is diagnostic of atmospheric water vapor between the sensor and the ground. This approach is frequently referred to as "split-window" since the two observations are contained in the same atmospheric radiance window. With the split-window approach ocean surface temperatures are generally estimated to within ±1.0°C of observed ocean surface temperatures (McClain et al. 1985).

Price (1983, 1984) proposed that split-window observations could also be used for land surface temperature measurements. He suggested a simple formulation:

$$T_s = T_4 + 3.33(T_4 - T_5), \tag{2}$$

where T_s = surface temperature (in degrees Celsius), T_4 = AVHRR channel 4 (10.3–11. 3 μm) brightness temperature (in degrees Celsius), and T_5 = AVHRR channel 5 (11.5–12.5 μm) brightness temperature (in degrees Celsius). Cooper and Asrar (1989) tested the validity of a variety of split-window approaches for estimating land surface temperatures for a grasslands region in the midwestern United States. They found that the Price (1984) approach generally produced estimates of surface temperatures to within ±3.0°C of ground measurements, for a constant 0.98 emissivity.

Material emissivity can introduce significant errors in estimating surface kinetic temperatures. When emissivity is not 1.0 and/or spectrally dependent several alternative approaches have been proposed to resolve the uncertainty introduced by emissivity variations (Price 1989, Wan and Dozier 1989, Becker and Li 1990). Accounting for emissivity variations, with only two TIR spectral measurements, requires independent information either about the observed landscapes or the atmospheric conditions during the observation. Information on landscape TIR emissivity patterns is relatively scarce (Prabhakara and Dalu 1976, Goward and Taranik 1986, Salisbury 1992). The best evidence suggests that most plant material emissivities are above 0.95, and when combined in canopy structures this increases to over 0.98 (Salisbury and D'Aria 1992). For the four western sites in Oregon (Fig. 1) the landscapes consisted of mostly closed vegetation canopies or thick understory litter. At sites 5 and 6 some bare soil was exposed under the plant canopies. Some minerals and soils display relatively low emissivity; for example, silica sands record values below 0.85 (Becker and Li 1990). The soils at the OTTER eastern sites originate from decay of geologically recent volcanic activity. There is little evidence that such volcanic materials have emissivities much less than 0.98 in the 10.3–12.5 μm spectral region. In the absence of specific knowledge concerning landscape emissivity patterns at the OTTER sites, we employed the Price (1984) approach with no emissivity adjustments.

Atmospheric humidity.—For the purpose of estimating atmospheric humidity, the fact that atmospheric water vapor attenuates TIR observations may be viewed as an asset rather than a liability. That is, the multispectral TIR observations may not only be used to estimate surface temperature but also to estimate the amount of water vapor in the intervening atmosphere (Dalu 1986, Jedlovec 1990, Kleespies and McMillin 1990, Justice et al. 1991). In essence, the measurement needed to derive accurate surface temperatures—atmospheric water vapor attenuation—also provides an estimate of the amount of water vapor between the sensor and the surface.

To date, studies have only investigated the relation between the split-window measurements and water vapor (precipatable water) in the entire column of the atmosphere between the sensor and the surface ($\approx$800 km depth by a 1.2 km^2 cross section, at nadir). In this study we were interested in comparing the split-window measurements with the water vapor in the lower portion of the atmosphere, surrounding the surface meteorological stations and the vegetation canopies. In general it does not appear feasible to derive surface humidity from these split-window measurements, at least when atmospheric conditions range from strong vertical mixing to thermal inversions (Dalu 1986). However, our interest was to evaluate midday atmospheric conditions, when, typically, surface heating produces strong vertical mixing in the boundary layer. Not only is the majority of atmospheric water vapor in the lower 1 km of the atmosphere but also during strong daytime vertical mixing this water vapor is generally well mixed in the active boundary layer. Under these conditions it seemed likely that a reasonable relation might be found between surface humidity conditions and the split-window measurements.

As in the derivation of accurate surface temperatures, the approach used to estimate atmospheric water vapor from split-window measurements requires consideration of special land conditions. Over land areas, where considerable spatial variation in surface temperature may occur, the difference in radiometric temperatures from the two spectral wavelengths varies, not only as a function of atmospheric water vapor, but also

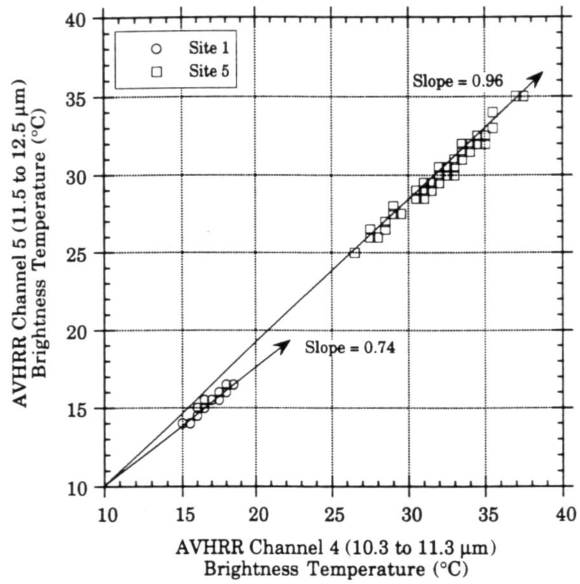

FIG. 2. Example of calculation of the slope of the relation between T_4 and T_5 observations to estimate atmospheric humidity. Observations are from 18 June 1990 for sites 1 and 5. The slope of the relation decreases as atmospheric humidity increases. T_4 = Advanced Very High Resolution Radiation (AVHRR) channel 4 (10.3–11.3 μm) brightness temperature (°C) and T_5 = AVHRR channel 5 (11.5–12.5 μm) brightness temperature (°C).

as a function of surface temperature. Kleespies and McMillin (1990) proposed the use of two observations, from targets of widely different temperatures, to account for the surface temperature factor. Jedlovec (1990) extended this approach to use of an array of observations. We followed the Jedlovec approach by calculating the least-squares slope relation between the two AVHRR radiometric temperatures—T_4 and T_5—from a 9 × 9 array of observations, centered on each of the study sites (Fig. 2). This slope varies inversely with atmospheric water vapor concentrations.

There were several underlying assumptions implicit in this analysis. First, the atmosphere was always experiencing strong vertical mixing. Second, atmospheric humidity during the observations was relatively uniform, horizontally, over the 81-km^2 region of the observations. In a well-mixed atmosphere this is more likely to be true. Third, as in the surface temperature calculations, emissivity did not vary with locations within or between sites. Assuming some success in this analysis, further consideration of these potential error sources must be undertaken.

To evaluate the validity of the split-window humidity estimates, we calculated the absolute humidity recorded at each meteorological observatory. Absolute humidity was calculated from the relative humidity

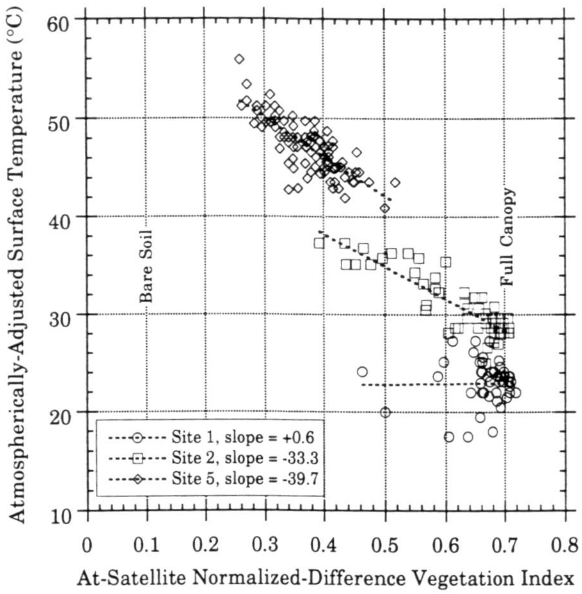

FIG. 3. Observed relation between NDVI (normalized-difference vegetation index) and surface temperature at sites 1, 3, and 5 on 13 July 1990. Low NDVI observations originate from locations with little vegetation cover. The surface temperature is therefore recording primarily the soil/litter background. The temperature of this surface varies with surface moisture. Lower surface temperatures are recorded as NDVI increases. Higher NDVI indicates more foliage cover. Extrapolation of NDVI to an "infinitely thick" canopy provides an estimate of foliar temperature that is generally comparable to air temperature.

and air temperature measured at the meteorological stations as follows (Sellers 1965, Rosenberg et al. 1983):

$$\chi = \frac{e_a M_m}{RT}, \tag{3}$$

where χ = absolute humidity (in grams per cubic metre), e_a = vapor pressure, M_m = molecular mass of water, R = universal gas constant, and T = absolute temperature. Absolute humidity is a measure of atmospheric water vapor in units of constant volume. Since it varies with atmospheric pressure (i.e., the same mass decreases in volume as pressure increases), it is not commonly used in meteorological work. However, remotely sensed observations record measurements from units of constant area (or volume in this case). Therefore absolute humidity is the relevant metric for comparison to satellite measurements. Further, given estimates of absolute humidity and air temperature it is then possible to solve for not only atmospheric vapor pressure but also vapor pressure deficit (which is also a function of air temperature).

There were two further limitations in the analysis carried out with OTTER observations. First, the EROS AVHRR TIR observations are processed to a 0.5°C radiometric precision, and are a factor of 5 lower than the original observations, which significantly reduces the precision of slope estimation for the relation between T_4 and T_5. Our use of the 9 × 9 data array for analysis may partially overcome this problem if the observed temperature range is relatively large. However, the original 0.1°C measurement precision would have been preferable. Second, the detectors used to measure relative humidity at OTTER degraded significantly during the observation period (see the *Appendix*). We developed a simple "gain-change" adjustment for these measurements to account for the lost sensitivity. Assessment of this adjustment required observations not available at the OTTER sites. In both cases these data quality problems introduced noise into the observations that restricted the quality of the results.

Air temperature and drought.—To estimate air temperature and environmental moisture conditions, we combined the atmospherically adjusted surface temperature (T_s) measurements with the normalized-difference vegetation index (NDVI) measurements. Evidence has accumulated that indicates that the combination of T_s and NDVI measurements is diagnostic of surface environmental conditions (Goward et al. 1985, Hope 1986, Goward and Hope 1989, Nemani and Running 1989, Carlson et al. 1990, Price 1990).

For any given remotely sensed observation, the TIR signal is simply an additive composite of the TIR emissions from background soils and overlying vegetation canopy (Fig. 3). The NDVI measurement is an estimate of the vegetation foliage cover. Typically observed TIR emissions decrease as the amount of foliage in the field of view of the sensor increases. This occurs because although plant canopies fill a considerable volume above land surfaces, their mass per unit volume is low. Whereas most radiant energy is absorbed by the full vegetation canopy, its heat capacity is little larger than air (Geiger 1965, Gates 1980). In contrast, soils, even dry sands, have much greater mass per unit volume than vegetation canopies, with a heat capacity an order of magnitude larger than vegetation canopies. As a result, during the daytime, soil surface temperatures in excess of 20°–30°C above air temperature are not unusual when the soils are dry. Vegetation canopy foliage, on the other hand, generally records temperatures within ±2°C of air temperature, with or without evapotranspiration taking place.

Air temperature may be estimated from the combined T_s and NDVI measurements by evaluating the recorded surface temperature of an "infinitely thick" vegetation canopy. Even in an array of observations that does not include "infinitely thick" canopy measurements, it is possible to estimate foliage temperature by simple extrapolation of the NDVI–T_s relation to the NDVI of an "infinitely" thick canopy. For most vegetation species this NDVI is ≈0.9 (Prihodko 1992).

Drought assessment was conducted by inspection of the slope of the relation between T_s and NDVI. For any given net radiation load, surface moisture conditions determine the temperature contrast between the soil surface and foliage. When the soil is dry it can rise to high temperatures. However, when the soil is wet all of the absorbed solar energy is used to evaporate the moisture and soil temperatures may consequentially approach or even fall below air temperature. Thus the slope of the NDVI–T_s relation varies in concert with surface wetness. How well this measure of surface wetness diagnoses ecosystem drought was a major objective of this study.

The same 9 × 9 observation array used for the atmospheric water vapor analysis is used in this step in the analysis. Nemani et al. (1993) have shown that this array size produces stable estimates of the relation observed between T_s and NDVI. The estimated canopy temperatures were compared to the shelter-height average air temperature collected at each meteorological station during the hour of the overpass. Drought was defined by observed increases in pre-dawn leaf water potential measurements (Runyon et al. 1994).

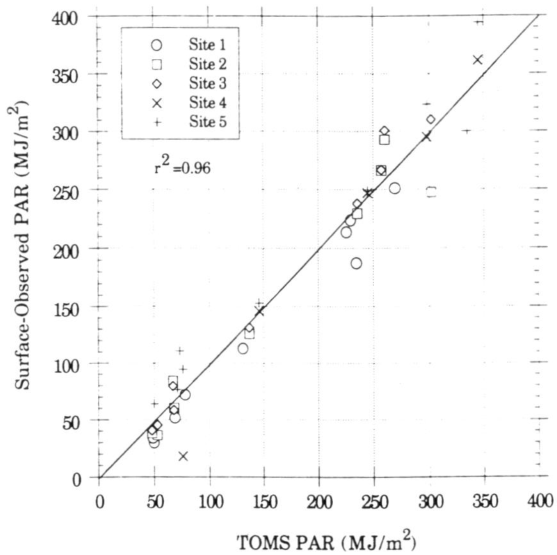

FIG. 4. Correlation between ground measurements and satellite estimates of monthly total incident PAR for five sites on the Oregon transect. Period of comparison: June 1989 to February 1990. Satellite estimates are from the TOMS (Total Ozone Mapping Spectrometer) sensor. Explained variance of the relation is >96%.

RESULTS AND DISCUSSION

Incident PAR

In general, the correspondence between surface-measured incident PAR (photosynthetically active radiation) and the TOMS (Total Ozone Mapping Spectrometer) estimate of this variable are excellent (Fig. 4). The explained variance of all comparable monthly observations (five sites, June 1989 to February 1990) is 96%, with root mean square error of ±22.7 MJ/m^2 and no bias (i.e., regression slope = 1.0). The TOMS measurements appear to provide a quite accurate estimate of incident PAR radiation patterns across the Oregon transect.

Some differences between the TOMS and ground-based measurements are evident (Fig. 5). In particular, the TOMS observations appear to overestimate incident PAR, in comparison to the ground measurements, at site 1. This discrepancy may occur because much of the TOMS observation is from the adjacent Pacific Ocean, or it may be the result of the placement of the meteorological observatory in a valley location surrounded by tall trees. Inclusion of the ocean surface may not present a realistic representation of cloud and fog frequency at this coastal location. The lack of a clear horizon for the radiation detector causes the early morning and late afternoon ground measurements to be lower than would be recorded at an open site. This difference becomes worse during the winter, which suggests that the ground site characteristics are the dominant cause of the differences observed at site 1.

No bias is observed between the ground and satellite measurements at any of the other OTTER sites. Explained variance ranges from 95% at site 2 to 99% at sites 3 and 4. There are departures between the two observations, particularly in midsummer and again in the winter. This may be related to variations in local cloud cover, which is most significant during those seasons of the year. When the ground measurements within a single TOMS grid cell (sites 2 and 3, 4 and 5) are averaged the relation to the TOMS observations is only slightly better, with a 2% increase in explained variance. This suggests that local variations in incident PAR occur within the TOMS grid cells, but that they are relatively small deviations from the regional patterns.

The TOMS observations successfully capture the basic character of the incident PAR environment in western Oregon, with incident PAR increasing from the coast to the interior deserts. If loss of local detail is acceptable then the TOMS measurements provide an excellent means to estimate incident PAR measurements, at least in western Oregon. Related work at other sites in the United States and selected other locations throughout the world has produced similar results (Dye 1992).

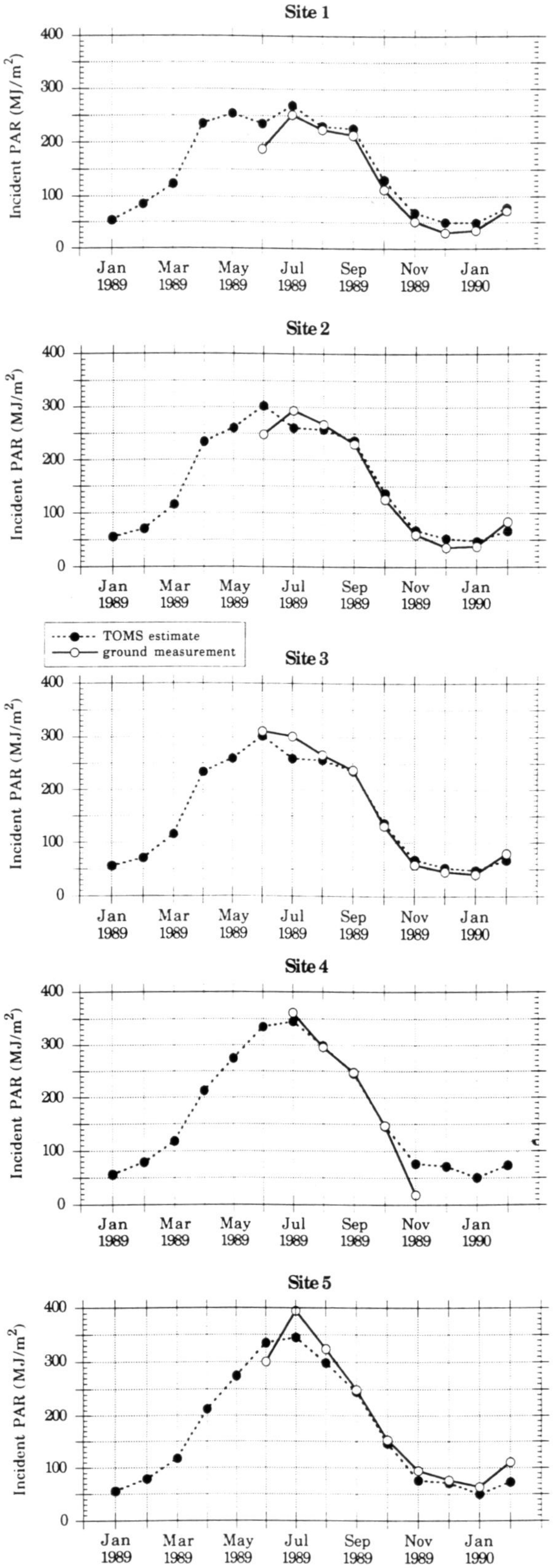

FIG. 5. Temporal comparison of monthly ground measurements and satellite estimates of incident PAR radiation. Departures between the observations appear to originate from local variations in incident radiation recorded by the ground sensors but lost in the relatively low spatial resolution of the TOMS sensor. The general correspondence is excellent but the satellite estimates consistently are larger than the ground measurements at site 1.

Intercepted PAR

AVHRR NDVI observations.—The advanced very high resolution radiometer (AVHRR) normalized-difference vegetation index (NDVI) observations capture the gradient of vegetation canopy conditions across the Oregon transect, with highest values to the west of the Cascades and lower values to the east (Fig. 6). However, the AVHRR observations suggest significant seasonal foliar dynamics, with relatively low NDVI values in the winter and higher values in the summer. This does not agree with measurements taken from the various aircraft instruments, which found little seasonal variation in spectral reflectance patterns across the transect (Spanner et al. 1994). The satellite observations are recording seasonal NDVI patterns not evident in the near-surface measurements.

The ultralight aircraft observations provide some evidence of the reasons for the AVHRR NDVI decrease in the winter. A quality set of ultralight measurements was collected from all sites in October 1990, nearly coincident with the AVHRR observations. Nevertheless, the July AVHRR observations compare more favorably with the ultralight measurements than the October AVHRR observations (Fig. 7). The deviations between the satellite and aircraft measurements are particularly large at sites 1–3.

Comparison of the visible wavelength measurements from the aircraft and satellite measurements (Fig. 8) indicates that the AVHRR observes a significant reflectance increase, at sites 1–3, in October. Visual inspection of the October AVHRR image revealed some fog at the coast and extensive burning in the Willamette Valley. These factors increase aerosol scattering, particularly in visible wavelengths (Fraser and Kaufman 1985), and therefore decrease NDVI. This same pattern of increased visible reflectance appears to remain throughout much of the winter season at sites 1–3. Insufficient atmospheric optical measurements were collected to confirm that a winter increase of aerosols causes the observed pattern (Spanner et al. 1994).

Seasonal and sequential variations in the near infrared AVHRR observations are also significant (Fig. 6). Variable concentrations of atmospheric water vapor

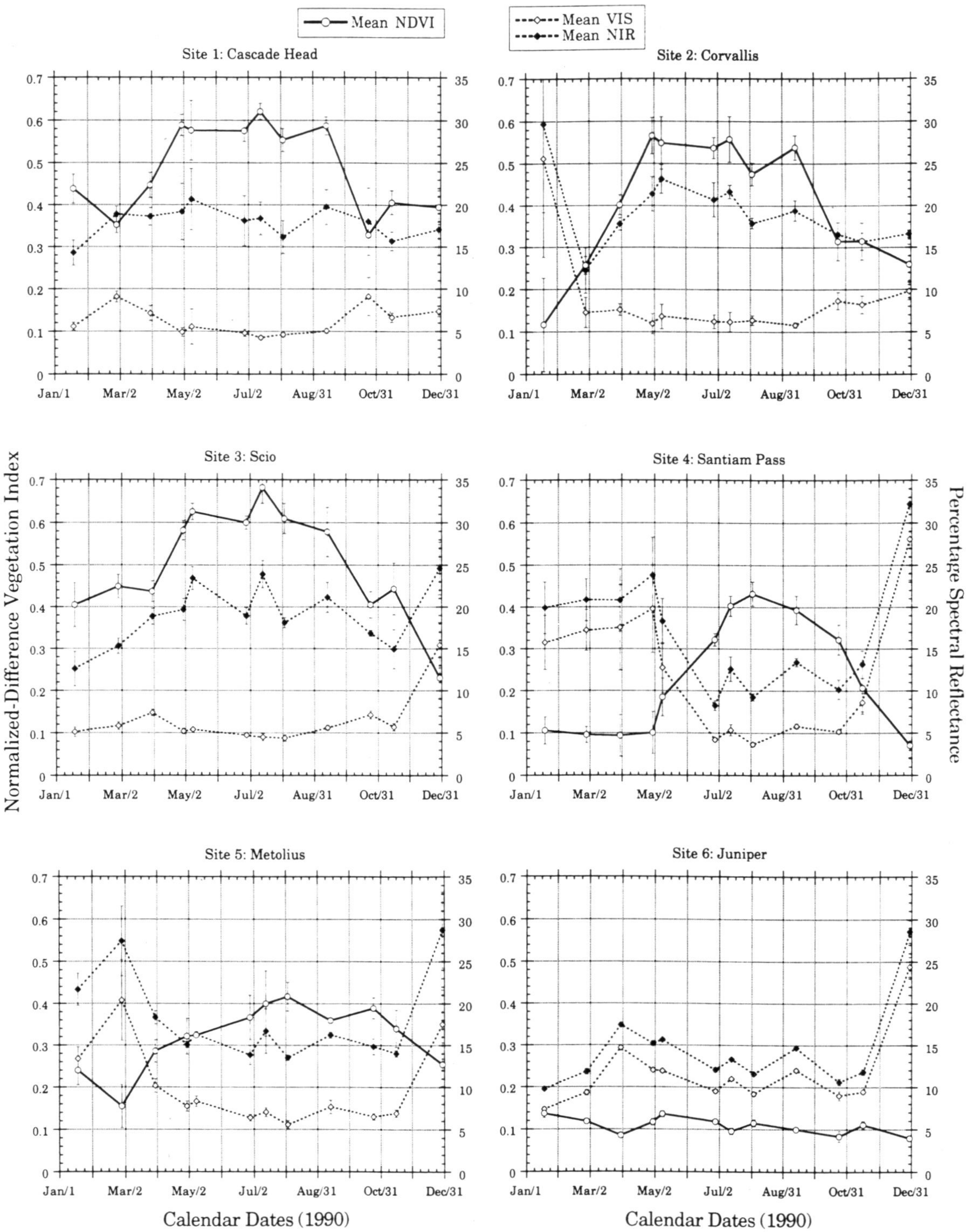

FIG. 6. Temporal plots of advanced very high resolution radiometer (AVHRR) normalized-difference vegetation index (NDVI) and of visible (VIS) and near-infrared (NIR) reflectance from OTTER sites for a 3 × 3 array of observations, centered on the geographic coordinates of each site. The vertical bars represent ±1 SD of the measurements. The high reflectances reported for sites 3–6 in December result from cloud contamination. The influence of snow is apparent at sites 4 and 5 during the winter. The seasonal patterns recorded at sites 1–3 may be strongly influenced by variations in atmospheric attenuation (see Fig. 7).

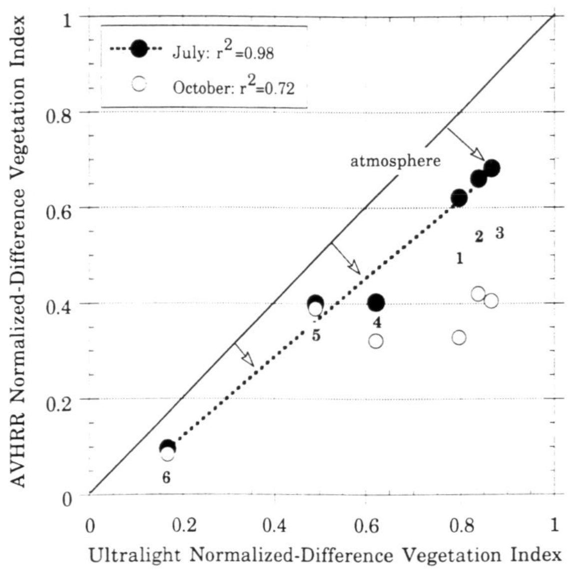

FIG. 7. Comparison of 1990 NDVI measurements from October ultralight observations with July and October AVHRR observations. Correspondence is generally good in July, but the AVHRR NDVI observed at sites 1–3 in October is much lower than the ultralight measurements. The reduction in measured NDVI from the satellite primarily occurs as a result of atmospheric attenuation. However, also note that the ultralight records a much higher NDVI at site 4 (Santiam Pass) than does the AVHRR. This is probably the result of surface heterogeneity in this mountainous region. The AVHRR observations record this variance, whereas the ultralight observations concentrated on more localized conditions.

may be a cause of these variations (Justice et al. 1991). In our comparison with the ground meteorological measurements we found little evidence of this linkage, although the difficulties encountered with the relative humidity sensors may have obscured the comparison. The observed variable reflectances also may have been caused by variable solar zenith angle and sensor view angle between dates (Table 1). The anisotropy of reflectance from vegetation canopies is well documented, and large variations in viewing conditions in the scenes examined could easily introduce this type of variable reflectance pattern (Kriebel 1978, Deering 1988).

The influence of snow is also apparent in the measurements. Background snow significantly alters NDVI measurements even when canopy LAI (leaf area index) does not change (Goward and Huemmrich 1992). At site 4 the observations from January to early May and again in November and December are dominated by background snow (Fig. 6). Snow cover also appears to be a factor at site 5 in January and February. The high December reflectances for sites 3, 4, 5, and 6 are primarily the result of cloud cover over the eastern portion of the transect.

In general, the summer observations from the AVHRR sensor record a reasonable representation of the surface NDVI variations in space and time. The satellite NDVI measurements are consistently lower than near-surface observations, indicative of atmospheric attenuation. Based on studies by Holben (1986) we have previously shown that a simple linear adjustment of the at-satellite NDVI, in the form

$$\mathrm{NDVI}_{\mathrm{surface}} = (1.1 \cdot \mathrm{NDVI}_{\mathrm{satellite}}) + 0.11 \tag{4}$$

produces a reasonable assessment of surface NDVI patterns (Goward et al. 1991). Application of this equation to the July AVHRR observations produced excellent agreement with the October ultralight observations (Fig. 9). Aircraft measurements recorded little variation in site NDVI values for four seasons of the year, so the agreement between July and October observations was expected (Spanner et al. 1994). The fit is particularly good for sites 1, 2, and 3. Sites 5 and 6 appear to be over-adjusted. This was probably because sites 5 and 6 are at 900 m above sea level, which results in less atmosphere between the sensor and the ground. The AVHRR records a lower NDVI at site 4 than the ultralight. This was probably the result of regional variations in surface conditions recorded by the AVHRR but not measured in the ultralight observations. Over-

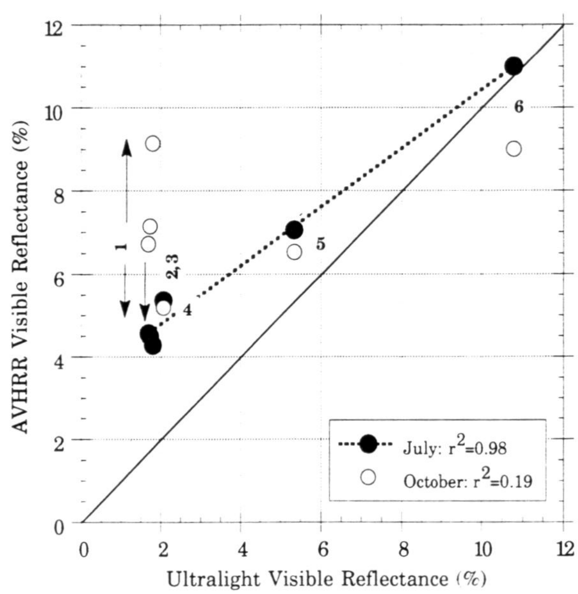

FIG. 8. Comparison of 1990 visible reflectance measurements from October ultralight observations with July and October AVHRR observations. Note the significant increase in visible reflectance at sites 1–3 observed by the AVHRR in October. Visual inspection of the image revealed fog at the coast and aerosol contamination from burning in the Willamette Valley. This is a major factor in the large decline in NDVI measurements observed by the AVHRR in October.

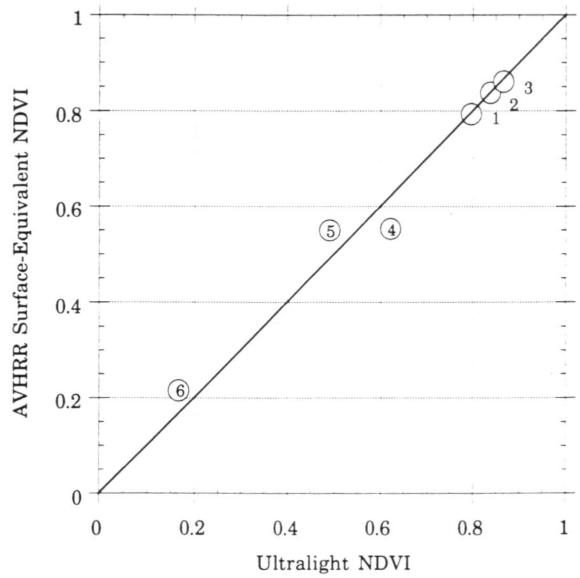

FIG. 9. Comparison of atmospherically adjusted July AVHRR NDVI observations with ultralight observations. The adjustment appears to work particularly well for sites 1–3. The over-adjustment at sites 5 and 6 is probably due to the increased elevation of these sites. The site 4 observations are discussed in the Fig. 7 legend.

all the explained variance in the relation is >97% with a root mean-square error (RMSE) of ±0.04 NDVI units and with a slight bias toward overprediction of the surface measurements from the adjusted satellite measurements.

AVHRR NDVI and IPAR.—With the exception of site 5, we found a strong relation between the ground-measured fractional IPAR and the July AVHRR NDVI measurements (Fig. 10). Excluding site 5, the regression estimate of this relation is

$$\%\mathrm{IPAR} = (121 \cdot \mathrm{NDVI}) - 4.0 \qquad (5)$$

with an explained variance of >99% with a RMSE of ±2.4% f_{IPAR} (fraction of canopy PAR intercepted). This fit agrees well with our estimate of this relation based on radiative transfer modeling (Goward and Huemmrich 1992). Inclusion of site 5 decreases the explained variance to 85% and increases the RMSE to ±13.6% f_{IPAR}. The discrepancy at site 5 is observed in both the AVHRR and the ultralight observations. This suggests that either the ground measurement is in error or that the remote-sensing observations are recording site characteristics not recorded in the ground observations. Site 5 has more substantial understory vegetation than the other sites, which was not observed in the ground f_{IPAR} measurements. Additional investigation at this site would be required to resolve this difference.

Combining TOMS incident PAR and AVHRR f_{IPAR}.—A combination of incident PAR and fractional IPAR is needed to estimate PAR captured by vegetation canopies and thus available for photosynthesis. In the case of the ground measurements, Runyon et al. (1994 [this issue]) multiplied monthly incident PAR measurements to fractional IPAR measured in midsummer. They held f_{IPAR} constant throughout the year (no change in canopy foliage), with the exception of the alder stands at site 1, and therefore tended to overestimate total annual IPAR available for photosynthesis. In the case of the AVHRR f_{IPAR} estimates the winter measurements are lower than expected, particularly at sites 1–3, because of increased atmospheric interference with the surface observations.

To evaluate the significance of these biases or errors, we computed a satellite estimate of annual IPAR for each site to compare with the ground estimates. Because the TOMS data were not available for all of 1990, we employed the 1989 monthly observations. The year-to-year variation in monthly total PAR is expected to be small, but this year discrepancy introduces another possible source of deviation between the ground and satellite measurements. The 1989 monthly TOMS incident PAR and 1990 AVHRR fractional IPAR values were multiplied and summed to annual values for comparison to the ground study. The TOMS observations

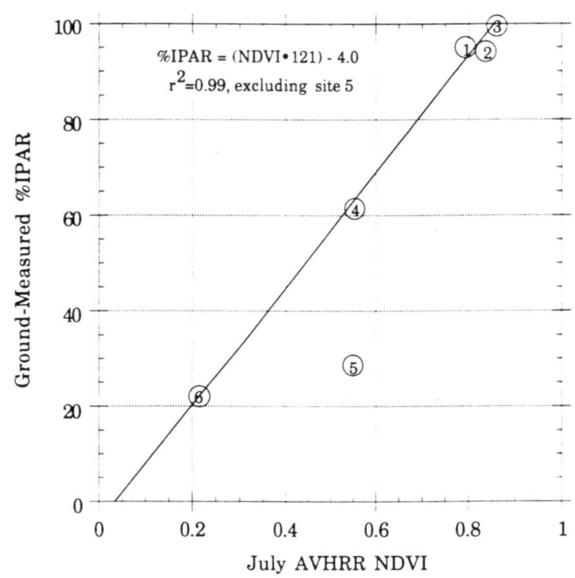

FIG. 10. Comparison of atmospherically adjusted July AVHRR NDVI measurements with ground measurements of percentage IPAR (% of the incident PAR that was intercepted). The deviation at site 5 may be the result of erroneous ground measurements. The ultralight observed the same discrepancy. Excluding site 5, the explained variance of the relation is >99%. The regression relation compares favorably with previous theoretical work.

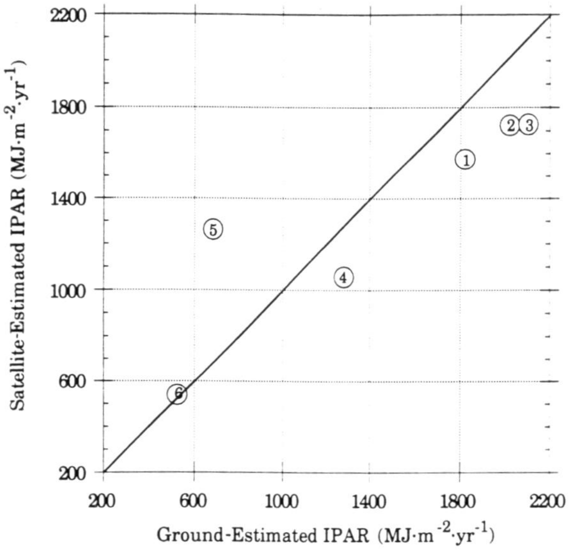

FIG. 11. Satellite vs. ground estimates of annual total intercepted photosynthetically active radiation (IPAR). Ground measurements are from under-canopy percentage IPAR and phyranometer observations. Satellite estimates are NDVI-estimated percentage IPAR and TOMS estimates in incident PAR. The deviation at site 5 results from the satellite percentage IPAR estimates, as discussed in the Fig. 10 legend.

for site 5 were also used for site 6. The results indicate that, with the exception of site 5, the satellite estimates are comparable to the ground estimates (Fig. 11). Excluding site 5, the explained variance is >99% with a RMSE of 58 MJ·m^{-2}·yr^{-1} (inclusion of site 5 reduces the explained variance to <80% with RMSE of 321 MJ·m^{-2}·yr^{-1}). There is, however, an observed bias; at sites 1–4 the satellite estimates are lower (400 MJ·m^{-2}·yr^{-1} lower at site 3) than the ground study found. Both the ground and satellite measurement errors must contribute to this difference. This agreement is better than might be expected given the errors encountered in the measurements. This occurs because the largest errors are encountered during the winter months when the incident solar flux is small.

Environmental variables

Atmospheric humidity.—We found a reasonably good correlation between shelter height absolute humidity and the slope of the relation between channels 4 and 5 thermal infrared (TIR) measurements (Fig. 12). The measurements also record the significant summer water vapor gradient from the coast to the interior high desert, which captures a basic constraint on growing conditions in western Oregon. Excluding outliers, the

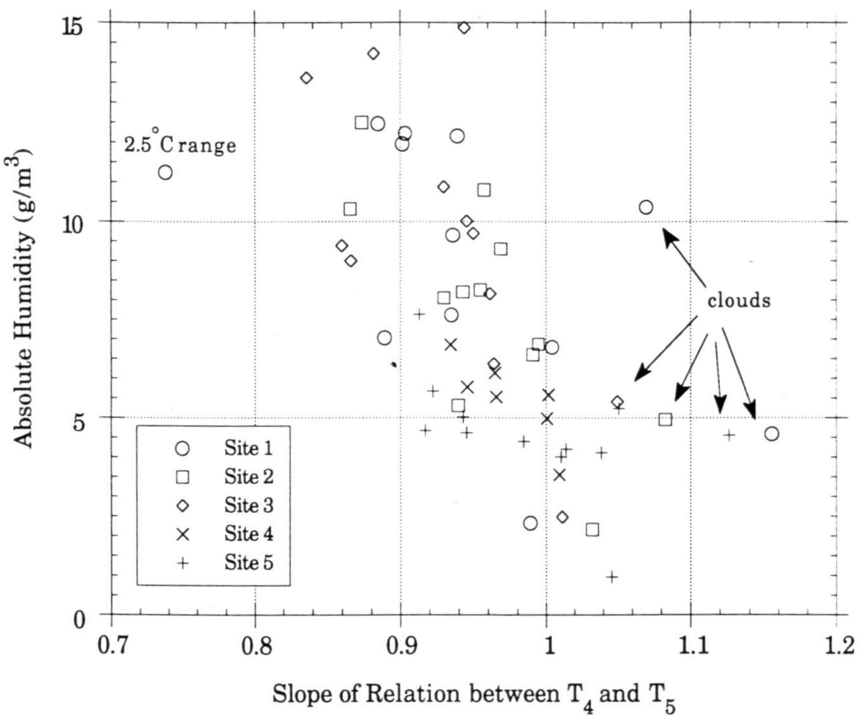

FIG. 12. Comparison of the slope of the relation between T_4 and T_5 observations and absolute humidity measured at the meteorological observatories. The basic pattern of high humidity in the west and lower humidity east of the Cascades is observed. However, the relation is quite noisy ($r^2 = 0.56$, excluding outliers). "Outliers" are noted on the diagram; they occur as a result of clouds and, for one point (at left), low measurement precision. The low explained variance probably results from the humidity instrument failure and the low precision of the EROS TIR measurements.

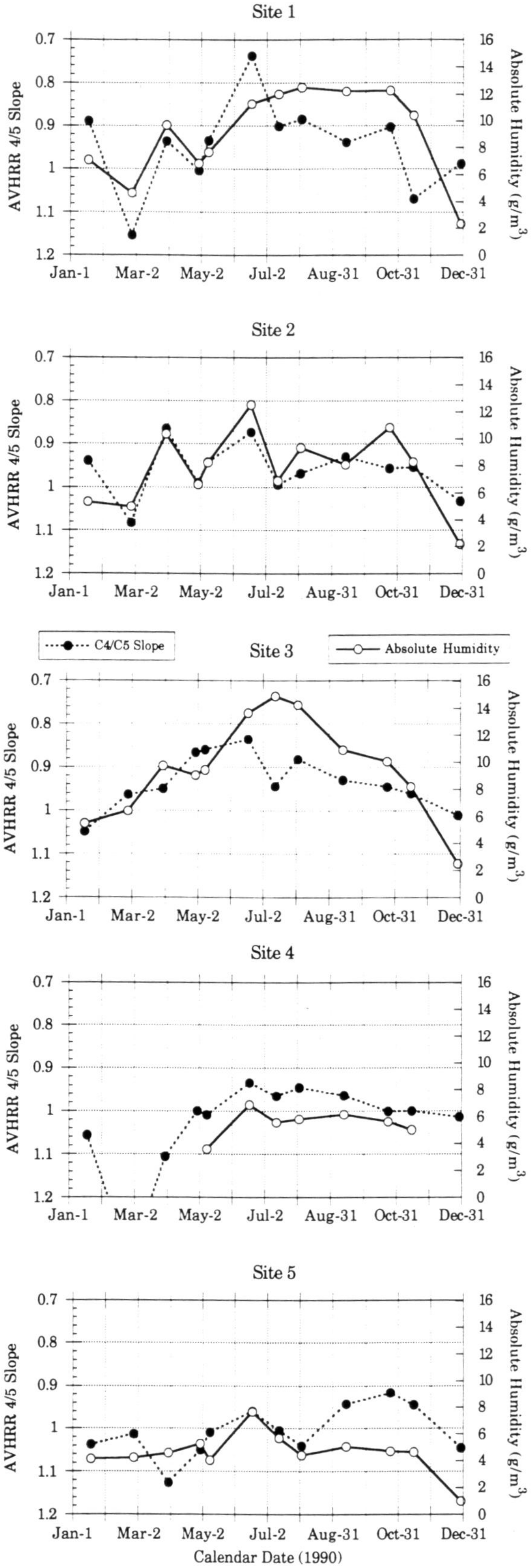

explained variance is better than 56% with a RMSE of 2.26 g/m^3. This level of measurement precision is relatively low, which suggests that either observations employed are relatively poor or the approach is wanting. The comparative seasonal variations in the ground and satellite measurements (Fig. 13) suggest that perhaps it is the failure of the ground instruments that is obscuring this analysis. At sites 1, 3, and 5 the two measurement sets diverge considerably in the latter half of the year. There was just insufficient information to pursue this problem within the context of the OTTER project.

There are some "outliers" in the relation between T_4 and T_5 (Fig. 12) that may originate either from insufficient data precision or presence of cloud contamination. The lowest slope measurement is derived from observations in which the observed total temperature range in the measurements is 2.5°C. For a data set with a 0.5°C precision, this is too small a range to estimate the slope of the relation with any precision. The presence of clouds was suggested when the slope is >1.0. When C5 (channel 5) records a larger temperature range than C4, the dominant TIR signal must originate from the atmosphere rather than the Earth's surface.

Given the previously stated conceptual and observation problems, the fact that a relation was found indicates that further investigation of this approach is warranted. A stronger relation should be achieved with higher precision AVHRR TIR measurements as well as better ground humidity measurements.

Air temperature.—The satellite-estimated air temperatures generally agree well with the ground-measured air temperature at the time of the overpass (Fig. 14). For all dates and sites ≈70% of the variance is captured in the satellite measurements, with a RMSE of ±5.4°C. This level of precision is less than desirable in the production-efficiency-model (PEM) calculations (see last paragraph of *Introduction,* above), but these results suggest that with further methodological development adequate measurement precision should be possible from the AVHRR observations.

There are a number of outliers in the satellite air temperature estimates. These can best be understood by examining the seasonal correspondence between the

←

FIG. 13. Temporal comparison of the slope of the relations between T_4 and T_5 observations and absolute humidity measured at the five OTTER sites. Departure of the two measurements as the season progresses suggests that humidity sensor failure is a primary cause of the "noise" in the observed relation. However, the satellite estimates also appear noisy, suggesting low measurement precision. Hopefully further tests of this concept will be carried out with better instruments and AVHRR data sets.

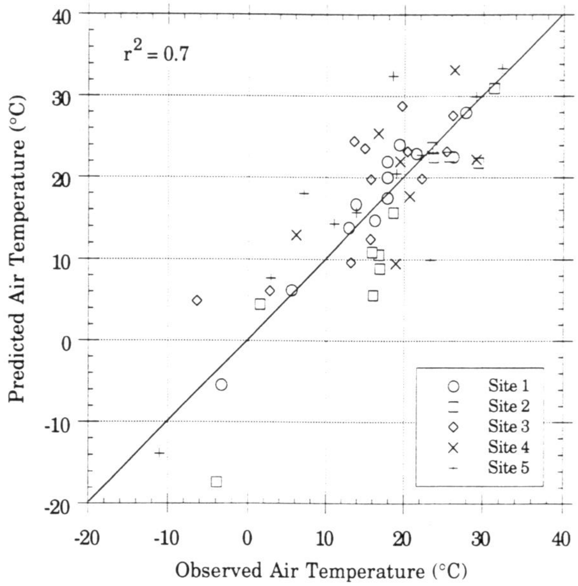

FIG. 14. Comparison of air temperature predicted from the NDVI/T_s relation vs. the air temperature observed at the meteorological stations. Explained variance is >70%. Predicted air temperatures are generally within ±3.0°C of the observed temperature. This is within the error associated with derivation of surface temperatures from the AVHRR observations. Outliers are discussed in Fig. 15.

ground measurements and satellite estimates (Fig. 15). At certain times, particularly during the winter, the satellite estimates deviate significantly from the ground estimates. This typically occurs when the slope of the NDVI/T_s relation is positive (Fig. 16) (T_s = surface temperature, in degrees Celsius), which suggests that either clouds are in the data array or there is snow underlying the forests (e.g., site 4). It is interesting to note that the positive slope does not always lead to large estimation errors. The observed slope is consistently positive or near zero at site 1 but the air temperature estimates are all within ±2°C of ground measurements.

Vapor pressure deficit from combined air temperature and absolute humidity.—In terms of the utilized PEM concept (Runyon et al. 1994 [this issue]) we were more interested in the capacity of the satellite observations to estimate atmospheric vapor pressure deficits (VPD)

→

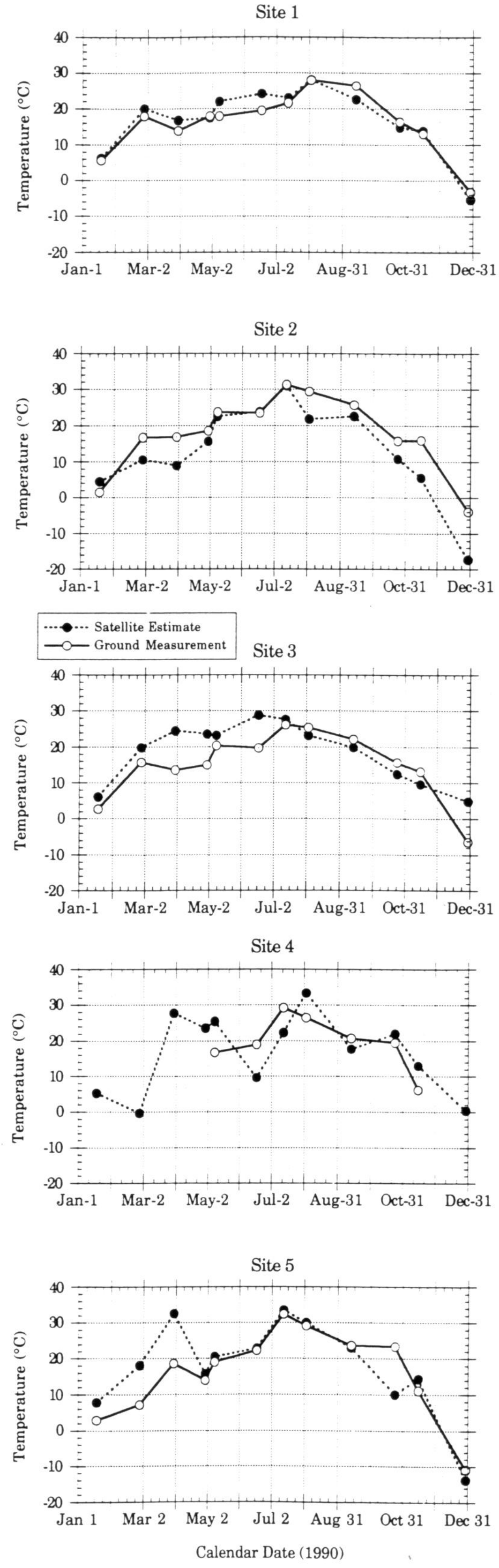

FIG. 15. Temporal comparison of the predicted vs. observed air temperature. The greatest errors occur in the winter and early summer when snow cover and cloud disrupt inference of surface cover from NDVI measurements (see Fig. 6). Further, the largest errors appear to occur when the regression-calculated slope of the relation is positive (see Fig. 17). The primary source of the errors appears to be inaccurate NDVI measurements.

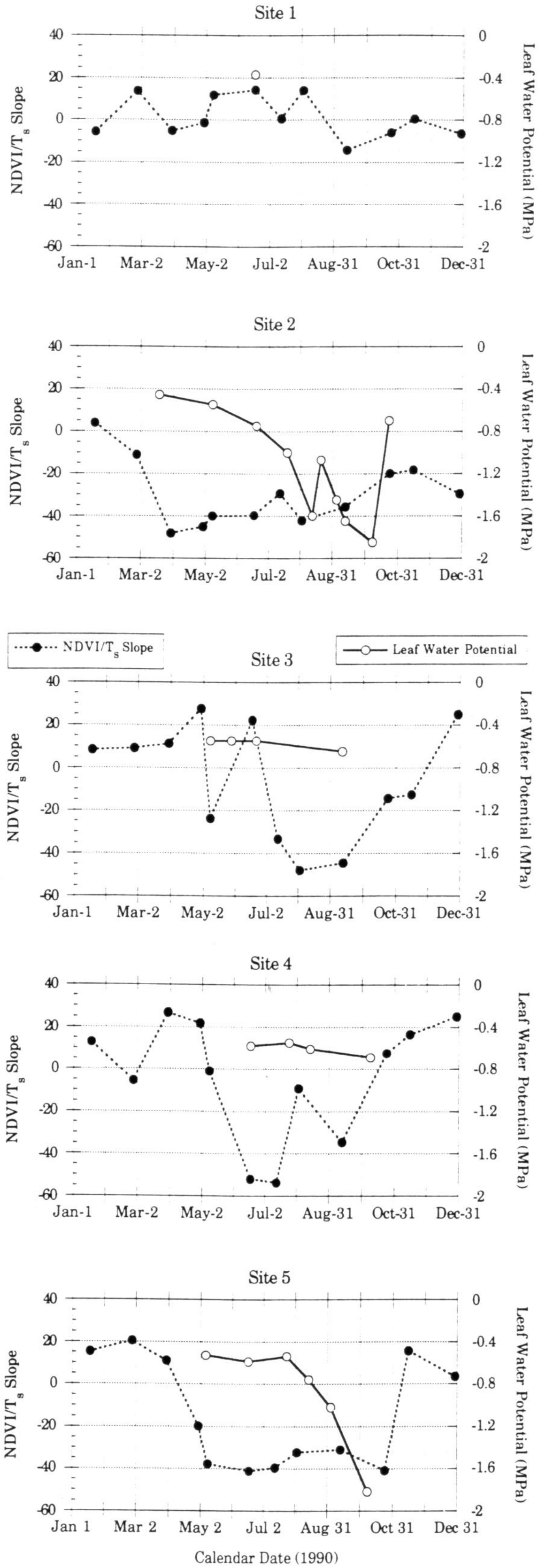

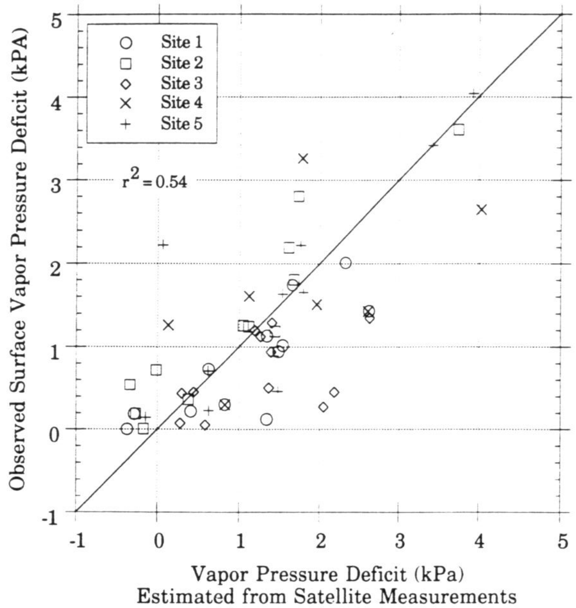

FIG. 17. Comparison of vapor pressure deficits evaluated from the meteorological station observations collected during the hour of the satellite overpass, with vapor pressure deficit (VPD) computed from the air temperature and absolute humidity estimates extracted from the satellite observations. Explained variance of the relation is >54%. The errors associated with the two parameters used to compute this vapor pressure deficit do not appear to be cumulative. That is, this explained variance is essentially equal to the error encountered in estimating absolute humidity. This suggests that considerable improvement in estimation of VPD may be possible with improved atmospheric humidity estimates.

than absolute humidity. VPD is a potential constraint on the use of IPAR for photosynthesis. Atmospheric vapor pressure may be calculated from absolute humidity and air temperature using Eq. 3. Saturation vapor pressure is a function of air temperature (Rosenberg et al. 1983). Vapor pressure deficit is simply the difference between saturation and atmospheric vapor pressure.

Using only the satellite estimates of air temperature and absolute humidity, we found that the satellite observations produced a reasonable approximation of VPD across all the sites and most dates (Fig. 17). For all sites and dates >54% of the variance in the ground measurements was captured in satellite estimates. The

←

FIG. 16. Temporal plots of the NDVI/T_s slope and leaf water potential measurements. The basic patterns of variable drought intensity across the OTTER sites is captured by the AVHRR observations. However, the AVHRR measurement shows a dry landscape (large negative slopes) 2–3 mo prior to the onset of plant drought recorded in the leaf water potential measurements.

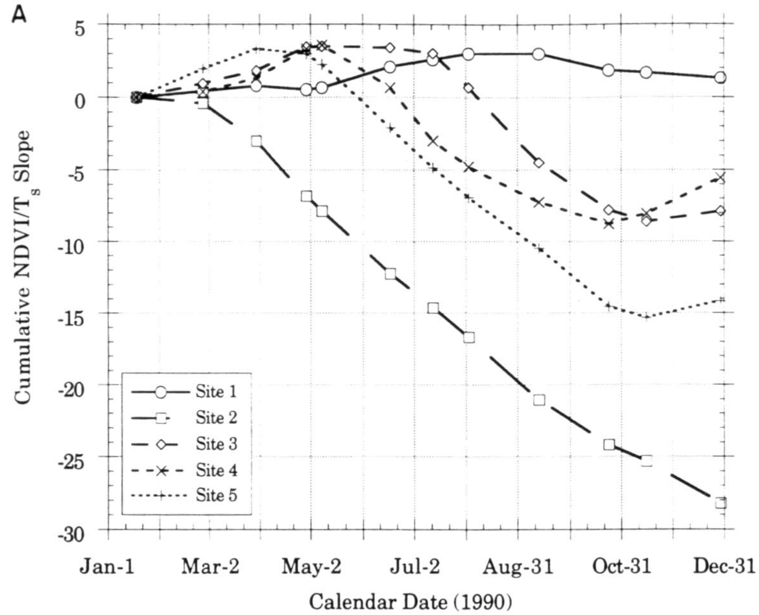

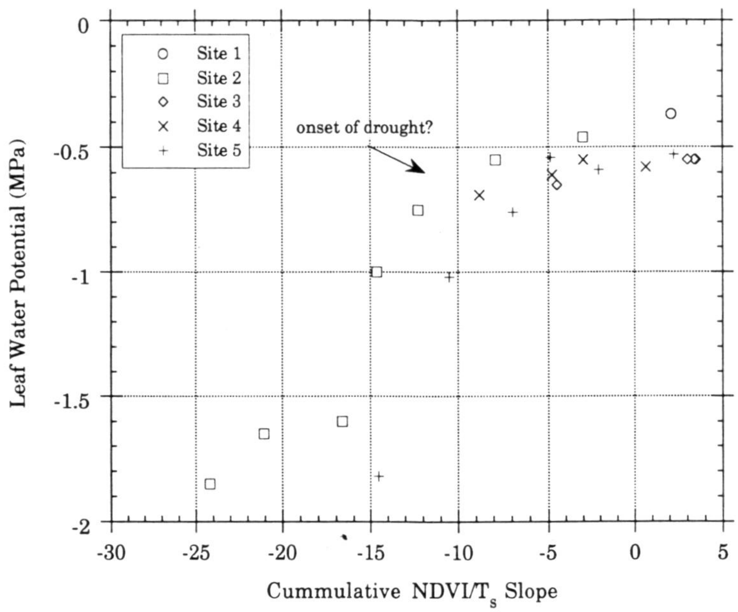

FIG. 18. (A) Time integration of the NDVI/T_s measurements (time step is days as percentage of year). This amplifies the contrasts in drought potential between sites as noted in Fig. 16. (B) Comparison of monthly leaf water potential measurements with the integrated NDVI/T_s slope measurements. Note that despite quite different seasonal timing of the onset of plant drought at the various sites, the cumulative satellite index appears to consistently track the onset of decreased leaf water potential measurements.

RMSE of the relation was ± 0.7 kPa, with little residual bias. Improved humidity estimates would clearly improve VPD estimates. The explained variance found here is essentially identical to that found for the absolute humidity alone. A measurement precision of better that ± 0.1 kPa would be desirable to meet the requirements of the utilized PEM model. These results suggest that with better quality satellite TIR observations (as well as ground measurements) this level of measurement precision is likely to be achieved.

Drought.—The comparison between plant drought, as measured by pre-dawn leaf water potential, and the slope of the NDVI/T_s relationship reveals an interesting pattern (Fig. 16). For the two sites (2 and 5) at which significant drought was measured, the decrease in leaf water potential occurs between 2 and 3 mo after the satellite observed a strong negative slope.

Despite the lag between plant drought and the satellite index, it does appear that when this index is accumulated (integrated) over the growing season (Fig. 18A) there is consistency between the length of dryness observed by the satellite and the onset of drought observed in the trees (Fig. 18B). This result suggests the remotely sensed observations are measuring surface moisture status whereas the plants access soil moisture reserves within the soil volume defined by rooting patterns.Thus, although the AVHRR satellite observations may not directly observe plant drought they provide a useful indicator of the surface moisture conditions that eventually lead to plant drought. Clearly, a simple hydrology model, which links soil moisture storage, plant water status, and the satellite measurements, would be of great value in conversion of the remotely sensed signals to information about plant drought (Wood et al. 1992).

Conclusions

This multidimensional test of satellite remote sensing as a source of ecological information has proven exceptionally fruitful. Despite the many limitations in the OTTER ground and satellite measurements, reasonable approximations of ecological and environmental conditions across the Oregon transect were extracted from the satellite measurements. The measurement precision found in this analysis was lower, for many of the variables, than might be desirable in many aspects of ecological research. However, within OTTER we found that a relatively simple model of production efficiency, constrained by simple environmental conditions, produced an effective description of variations in primary production across the Oregon transect (Runyon et al. 1994). Results from this analysis of the satellite observations indicate that, with further modest refinements, the requirements of the PEM approach could be met with the satellite observations.

The simplest improvement that can be accomplished in the satellite observations is preservation of the 10-bit measurement precision during data processing. This is a particularly critical issue in the thermal infrared (TIR) observations, where small observed variations are diagnostic of relatively large changes in surface environmental conditions. A more difficult problem encountered in this analysis was the impact of variable atmospheric attenuation and residual cloud cover on surface measurement accuracy. Further conceptual and analytical developments in the separation of atmospheric and surface signals in remotely sensed measurements is sorely needed. Recent progress in this direction is encouraging (Kaufman and Sendra 1988, Rossow et al. 1989, Goa and Goetz 1990, Stowe et al. 1991), but implementation of many of these concepts will require more sophisticated observatories than exist today.

The advent of more sophisticated sensors in the near future (e.g., the NASA Earth Observing System) should include the complement of additional measurements and precision needed to extract the desired measurement accuracy. There is also considerably more progress that may be accomplished with existing remote-sensing observatories. This study considers only two sensor systems. Inclusion of measurements from satellite systems such as the Geostationary Operational Environmental Satellite (GOES), which provides half-hour updates of surface conditions (Yates et al. 1986) and passive microwave observations from instruments such as the Scanning Multichannel Microwave Radiometer (SMMR) (Njoku 1982, Choudhury 1989) might provide additional, complementary ecological information.

One issue in particular will require further attention before satellite observations can serve as major reliable sources for environmental measurements. The estimates of air temperature and atmospheric humidity presented here represent comparisons between essentially instantaneous measurements. Since the satellite observations can only provide periodic updates of these variables (e.g., once every 2 wk) methods must be developed to extrapolate, both diurnally and daily, between these observations. Extrapolation requires knowledge of the magnitude and duration of cloud cover. The AVHRR acquires daily observations but, in terrestrial research, the cloud-contaminated scenes are most often not examined. A truly effective satellite-based ecological monitoring system should incorporate all acquired observations to produce, daily, either estimates of surface conditions in cloud-free observations, or estimates of atmospheric (and therefore surface) conditions during periods of cloud cover.

This study indicates that it is possible, though not necessarily easy, to extract critical ecological and environmental information from satellite remotely sensed observations. In concert with the results from the field analysis (Runyon et al. 1994) this study suggests that monitoring the state and functioning of ecosystems is possible with remote sensing. The results point out the pressing need to develop better methods for cloud detection and for accounting for variable atmospheric attenuation in satellite observations. Nevertheless, perhaps the most exciting prospect is that the potential exists today to extract global patterns of these ecological variables for comparison with field studies at sites throughout the globe. Such a global effort should lead to rapid refinement of not only these remote-sensing methods but also improved descriptions of global patterns of ecosystem dynamics.

ACKNOWLEDGMENTS

This study was conducted with the support of the National Science Foundation and the National Aeronautics and Space Administration. NSF support originated from grant BSR-8905278 (to S. N. Goward). NASA support was from grant NAGW-1152 (to S. N. Goward) and NAGW-1717 (to R. H. Waring).

In addition, Mr. Jeff Eidenshenk, EROS Data Center, provided significant assistance with acquisition of the AVHRR observations. Dr. Ralph Dubayah and Mr. Derak Pross supplied important input to the atmospheric water vapor analysis. Mr. John Runyon and Mr. Rich McCreight assisted in provision of the ground meteorological observations and instrument specifications.

LITERATURE CITED

Asrar, G., editor. 1989. Theory and applications of optical remote sensing. John Wiley & Sons, New York, New York, USA.

Asrar, G., M. Fuchs, E. T. Kanemasu, and J. L. Hatfield. 1984. Estimating absorbed photosynthetic radiation and leaf area index from spectral reflectance in wheat. Agronomy Journal **76**:300–306.

Becker, F., and Z. Li. 1990. Towards a local split window method over land surfaces. International Journal of Remote Sensing **11**:369–393.

Bray, J. M. 1966. The visible albedo of surfaces in central Minnesota. Ecology **47**:524–531.

Brest, C. L., and S. N. Goward. 1987. Deriving surface albedo measurements from narrow band satellite data. International Journal of Remote Sensing **8**:351–367.

Carlson, T. N., E. M. Perry, and T. J. Schmugge. 1990. Remote estimation of soil moisture availability and fractional vegetation cover for agricultural fields. Agricultural and Forest Meteorology **52**:45–69.

Choudhury, B. J. 1987. Relationships between vegetation indices, radiation absorption and net photosynthesis evaluated by a sensitivity analysis. Remote Sensing of Environment **22**:209–233.

———. 1989. Monitoring global land surface using NIMBUS-7 37 GHz polarization difference. International Journal of Remote Sensing **10**:1579–1605.

Cooper, D. I., and G. Asrar. 1989. Evaluating atmospheric correction models for retrieving surface temperatures from the AVHRR over a tallgrass prairie. Remote Sensing of Environment **27**:93–102.

Dalu, G. 1986. Satellite remote sensing of atmospheric water vapor. International Journal of Remote Sensing **7**:1089–1097.

Daughtry, C. S. T., K. D. Gallo, and M. E. Bauer. 1983. Spectral estimates of solar radiation intercepted by corn canopies. Agronomy Journal **75**:527–531.

Deering, D. W. 1988. PARABOLA directional field radiometer for aiding in space sensor data interpretation. Pages 249–261 *in* Recent advances in sensors, radiometry, and data processing for remote sensing. Society of Photo-Optical Instrumentation Engineers, New York, New York, USA.

Deschamps, P. Y., and T. Phulpin. 1980. Atmospheric correction of infrared measurements of sea surface temperature using channels at 3.7 μm, 11, and 12 μm. Boundary Layer Meteorology **18**:131–143.

Dickinson, R. E. 1984. Modelling evapotranspiration for three dimensional global climate models. Pages 58-72 *in* Climate processes and climate sensitivity. Monograph. American Geophysical Union, Washington, D.C., USA.

Dye, D. G. 1992. Satellite estimation of global distribution and variability of incident photosynthetically active radiation. Dissertation. Department of Geography, University of Maryland, College Park, Maryland, USA.

Eck, T., F. Bhartia, P. K. Hwang, and L. L. Stowe. 1987. Reflectivity of the Earth's surface and clouds in ultraviolet wavelengths from satellite observations. Journal of Geophysical Research **92**:4287–4296.

Eck, T., and D. Dye. 1991. Satellite estimation of photosynthetically active radiation at the Earth's surface. Remote Sensing of Environment **38**:135–146.

Eidenshenk, J. 1992. The 1990 coterminous U.S. AVHRR data set. Photogrammetric Engineering and Remote Sensing **58**:809–813.

Field, C. B. 1991. Ecological scaling of carbon gain to stress and resource availability. Pages 35–65 *in* H. A. Mooney, W. E. Winner, and E. J. Pell, editors. Response of plants to multiple stresses. Academic Press, New York, New York, USA.

Fraser, R. S., and Y. J. Kaufman. 1985. The relative importance of scattering and absorption in remote sensing. IEEE Transactions in Geosciences and Remote Sensing **23**:625–633.

Gates, D. M. 1980. Biophysical ecology. Springer-Verlag, New York, New York, USA.

Geiger, R. 1965. Climate near the ground. Revised edition (translated from German). Harvard University Press, Cambridge, Massachusetts, USA.

Goa, B. C., and A. F. Goetz. 1990. Column atmospheric water vapor and vegetation liquid water retrievals from airborne imaging spectrometer data. Journal of Geophysical Research **95**:3549–3564.

Goward, S. N. 1989. Satellite bioclimatology. Journal of Climate **7**:710–720.

Goward, S. N., G. C. Cruickshanks, and A. S. Hope. 1985. Observed relation between thermal emissions and reflected spectral reflectance from a complex vegetated landscape. Remote Sensing of Environment **18**:137–146.

Goward, S. N., and D. G. Dye. 1987. Evaluating North American net primary productivity with satellite observations. Advances in Space Research **7**(11):165–174.

Goward, S. N., and A. S. Hope. 1989. Evapotranspiration from combined reflected solar and emitted terrestrial radiation: preliminary FIFE results from AVHRR data. Advances in Space Research **9**:239–249.

Goward, S. N., and K. F. Huemmrich. 1992. Vegetation canopy PAR absorptance and the normalized difference vegetation index: an assessment using the SAIL model. Remote Sensing of Environment **39**:119–140.

Goward, S. N., A. Kerber, D. G. Dye, and V. Kalb. 1987. Comparison of North and South American biomes from AVHRR observations. Geocarto **2**:27–40.

Goward, S. N., B. Markham, D. G. Dye, W. Dulaney, and J. Yang. 1991. Normalized difference vegetation index measurements from advanced very high resolution radiometer. Remote Sensing of Environment **35**(2 and 3):259–279.

Goward, S. N., and J. V. Taranik, editors. 1986. Commercial applications and scientific research requirements for thermal infrared observations of terrestrial surfaces. TIR Working Group report to National Aeronautics and Space Administration and Earth Observation Satellite Company. Earth Satellite Observation Company, Lanham, Maryland, USA.

Goward, S. N., C. J. Tucker, and D. G. Dye. 1985. North American vegetation patterns observed with the NOAA-7 advanced very high resolution radiometer. Vegetatio **64**:3–14.

Heimann, M., and C. D. Keeling. 1989. A three-dimensional model of atmospheric CO_2 transport based on observed winds. 2. Model description and simulated experiments. Geophysical Monograph **55**:237–275.

Holben, B. N. 1986. Characteristics of maximum-value composite images from temporal AVHRR data. International Journal of Remote Sensing **7**:1417–1434.

Holben, B. N., Y. J. Kaufman, and J. D. Kendall. 1990. NOAA-11 AVHRR visible and near-IR inflight calibration. International Journal of Remote Sensing **11**:1511–1519.

Hope, A. S. 1986. Estimating evapotranspiration from combined spectral reflectance and thermal emissions data. Dissertation. Department of Geography, University of Maryland, College Park, Maryland, USA.

Hwang, P. H., L. L. Stowe, H. Y. M. Yeh, and H. L. Kyle. 1988. The Nimbus-7 global cloud climatology. Bulletin of the American Meteorological Society **69**:743–752.

Jarvis, P. G. 1981. Production efficiency of coniferous forest in the U.K. Pages 81–107 *in* C. B. Johnson, editor. Physiological processes limiting productivity. Butterworth, London, England.

Jedlovec, G. J. 1990. Precipitable water estimation from high-resolution split window radiance measurements. Journal of Applied Meteorology **29**:863–877.

Justice, C. O., T. Eck, D. Tanre, and B. N. Holben. 1991. The effect of water vapor on the normalized difference vegetation index derived for the Sahelian Region from NOAA AVHRR data. International Journal of Remote Sensing **12**: 1165–1188.

Justice, C. O., J. R. G. Townshend, B. N. Holben, and C. J. Tucker. 1985. Analysis of the phenology of global vegetation using meteorological satellite data. International Journal of Remote Sensing **6**:1271–1381.

Kaufman, Y. J., and C. Sendra. 1988. Algorithm for automatic atmospheric corrections to visible and near-IR satellite data. International Journal of Remote Sensing **9**:1357–1381.

Kerr, J. P., G. W. Thurtell, and C. B. Tanner. 1967. An integrating pyranometer for climatological observer stations and mesoscale networks. Journal of Applied Meteorology **6**:688–694.

Kidwell, K. B. 1988. NOAA polar orbital data user's guide. NOAA National Climate Data Center, World Weather Building, Suitland, Maryland, USA.

Kleespies, T. J., and L. M. McMillin. 1990. Retrieval of precipitable water from observations on split window over varying surface temperatures. Journal of Applied Meteorology **29**:851–862.

Koomanoff, V. A. 1989. Analysis of global vegetation patterns: a comparison between remotely sensed data and a conventional map. Biogeography Research Series Report 890201. Department of Geography, University of Maryland, College Park, Maryland, USA.

Kriebel, K. T. 1978. Measured spectral bidirectional reflection properties of four vegetation surfaces. Applied Optics **17**:253–259.

Kumar, M., and J. L. Monteith. 1982. Remote sensing of plant growth. Pages 134–144 *in* H. Smith, editor. Plants and the daylight spectrum. Pitman, London, England.

Landsberg, J. L. 1986. Physiological ecology of forest production. Academic Press, London, England.

Loveland, T. R., J. W. Merchant, D. O. Ohlen, and J. F. Brown. 1991. Development of a land-cover characteristics database for the coterminous U.S. Photogrammetric Engineering and Remote Sensing **57**:1453–1463.

McClain, E. P., W. G. Pichel, and C. C. Walton. 1985. Comparative performance of AVHRR-based multichannel sea surface temperatures. Journal of Geophysical Research **90**: 11587–11601.

Monteith, J. L. 1977. Climate and efficiency of crop production in Britain. Philosophical Transactions of the Royal Society, Series B **281**:277–294.

Monteith, J. L., and M. H. Unsworth. 1990. Principles of environmental physics. Second edition. Edward Arnold, London, England.

Mooney, H., and R. Hobbs, editors. 1990. Remote sensing of biospheric functioning. Springer-Verlag, New York, New York, USA.

Nemani, R., L. Pierce, S. Running, and S. N. Goward. 1993. Developing satellite-derived estimates of surface moisture status. Journal of Applied Meteorology **32**:548–557.

Nemani, R. R., and S. W. Running. 1989. Estimation of surface resistance to evapotranspiration from NDVI and thermal-IR AVHRR data. Journal of Climate and Applied Meteorology **28**:276–294.

Njoku, E. G. 1982. Passive microwave remote sensing of the earth from space—a review. Proceedings of Institute for Electrical and Electronics Engineers **70**:728–750.

Peterson, D. L., and R. H. Waring. 1994. Overview of the Oregon Transect Ecosystem Research project. Ecological Applications **4**:211–225.

Pinker, R. T., and I. Laszlo. 1992. Global distribution of photosynthetically active radiation as observed from satellites. Journal of Climate **5**:56–65.

Prabhakara, C., and G. Dalu. 1976. Remote sensing of surface emissivity at 9 μm over the globe. Journal of Geophysical Research **81**:3719–3724.

Prabhakara, C., V. G. Dalu, and V. G. Kunde. 1974. Estimation of sea surface temperature from remote sensing in the 11–13 μm window range. Journal of Geophysical Research **79**:5039–5044.

Price, J. C. 1983. Estimating surface temperatures from satellite thermal infrared data—a simple formulation for the atmospheric effect. Remote Sensing of Environment **13**: 353–361.

———. 1984. Land surface temperature measurements from the split window channels of the NOAA 7 advanced very high resolution radiometer. Journal of Geophysical Research **89**(D5):7231–7237.

———. 1989. Quantitative aspects of remote sensing in the thermal infrared. Pages 578-603 *in* G. Asrar, editor. Theory and applications of optical remote sensing. John Wiley & Sons, New York, New York, USA.

———. 1990. Using spatial context in satellite data to infer regional scale evapotranspiration. Institute for Electrical and Electronics Engineers Transactions on Geosciences and Remote Sensing **28**:940–948.

Prihodko, L. 1992. Estimation of air temperature from remotely sensed observations. Thesis. Department of Geography, University of Maryland, College Park, Maryland, USA.

Prince, S. D., S. N. Goward, D. G. Dye, and C. S. Daughtry. 1990. Models of remote sensing of primary production at the regional and global scales. Pages 559–562 *in* R. Mills, editor. Tenth International Geoscience and Remote Sensing Symposium, College Park, Maryland. Institute of Electrical and Electronic Engineers, New York, New York, USA.

Rosenberg, N. J., B. L. Blad, and S. B. Verma. 1983. Microclimate: the biological environment. Second edition. John Wiley & Sons, New York, New York, USA.

Rossow, W. B., L. C. Garder, and A. A. Lacis. 1989. Global seasonal cloud variations from satellite radiance measurements. 1. Sensitivity analysis. Journal of Climate **2**:214–247.

Running, S. W., and J. C. Coughlan. 1988. A general model of forest ecosystem processes for regional applications. I. Hydrologic balance, canopy gas exchange and primary production processes. Ecological Modelling **42**:125–154.

Running, S. W., R. R. Nemani, and R. D. Hungerford. 1987. Extrapolation of synoptic meteorological data in mountainous terrain and its use for simulating forest evapotranspiration and photosynthesis. Canadian Journal of Forestry Research **17**:472–483.

Runyon, J., R. H. Waring, S. N. Goward, and J. M. Welles. 1994. Environmental limits on net primary production and light-use efficiency across the Oregon transect. Ecological Applications **4**:226–237.

Salisbury, J. W., guest editor. 1992. Temperature and emissivity separation. Special issue. Remote Sensing of Environment **42**:82–165.

Salisbury, J. W., and D. M. D'Aria. 1992. Emissivity of terrestrial materials in the 8–14 μm atmospheric window. Remote Sensing of Environment **42**:83–106.

Schneider, S. R., and D. F. McGinnis, Jr. 1982. The NOAA AVHRR: a new sensor for monitoring crop growth. Pages 223–230 *in* Machine processing of remotely sensed data. Purdue University, West Lafayette, Indiana, USA.

Sellers, P. J. 1985. Canopy reflectance, photosynthesis, and transpiration. International Journal of Remote Sensing **6**: 1335–1371.

Sellers, P. J., Y. Mintz, Y. C. Sud, and A. Dalcher. 1986. A simple biosphere model (SiB) for use with general circulation models. Journal of Atmospheric Sciences **43**:505–531.

Sellers, W. D. 1965. Physical climatology. University of Chicago Press, Chicago, Illinois, USA.

Spanner, M. A., L. Johnson, J. Miller, R. McCreight, J. Freemantle, J. Runyon, and P. Gong. 1994. Remote sensing of seasonal leaf area index across the Oregon transect. Ecological Applications **4**:258–271.

Stoner, E. R., and M. F. Baumgardner. 1981. Characteristic variations in reflectance of surface soils. Soil Science Society of America Journal **45**:1161–1165.

Stowe, L. L., E. P. McClain, R. Carey, P. Pellegrino, G. Gutman, P. Davis, C. Long, and S. Hart. 1991. Global distribution of cloud cover dervied from NOAA/AVHRR operational satellite data. Advances in Space Research **3**:51–54.

Swain, P. H., and S. M. Davis, editors. 1978. Remote sensing: the quantitative approach. McGraw-Hill, New York, New York, USA.

Townshend, J. R. G., C. O. Justice, W. Li, C. Gurney, and J. McManus. 1991. Global land cover classification by remote sensing: present capabilities and future possibilities. Remote Sensing of Environment **35**:243–255.

Tucker, C. J., I. Y. Fung, C. D. Keeling, and R. H. Gammon. 1986. Relationship between atmospheric CO_2 variation and a satellite-derived vegetation index. Nature **319**:195–199.

Tucker, C. J., J. R. G. Townshend, and T. E. Goff. 1985. African land-cover classification using satellite data. Science **227**:369–375.

Wan, Z., and J. Dozier. 1989. Land surface temperature measurement from space. Institute for Electrical and Electronics Engineers Transactions on Geosciences and Remote Sensing **27**: 268–278.

Wolfe, W. L., editor. 1965. Handbook of military infrared technology. Office of Naval Research, Department of the Navy, Washington, D.C., USA.

Wood, E. F., D. P. Lettenmaier, and J. Zartarian. 1992. A land-surface hydrological parameterization with subgrid variability for general circulation models. Journal of Geophysical Research **97**:2717–2728.

Yates, H., A. Strong, D. McGinnis, Jr., and D. Tarpley. 1986. Terrestrial observations from NOAA operational satellites. Science **231**:463–470.

APPENDIX

Relative Humidity Measurements at OTTER

We experienced a significant instrument failure in the surface meteorological measurements acquired for OTTER. The observatories, as acquired from Campbell Scientific Instruments, Inc. (Logan, Utah, USA) included a "phys-chemical research PCRC-11 RH sensor." As noted in the instrument manual, "In a clean air environment, the PCRC-11 chip should perform reliably for up to one year when housed in CSI's 041 sensor shelter. The chip is easily replaced in the event of failure."

Given other commitments, we paid little attention to the accumulating meteorological measurements until mid-1990. Having deployed the meteorological stations in June 1989, it seemed reasonable to expect that the sensors would all perform reliably until at least mid-1990. With considerable dismay, we discovered that the relative humidity sensors had begun to degrade, as quickly as 1 mo (site 3) after deployment (Fig. A1). Staff (R. McCreight) had noticed that material was flaking from the PCRC-11 chip when he visited the stations to download the monthly observations, but had thought little about its significance until we examined the cumulative data record. In fact, the relative humidity sensors at all of the sites began to decay not later than 6 mo following deployment.

This instrument failure creates a rather knotty problem for a variety of the research objectives in OTTER. Vapor pressure deficits are a primary control on photosynthesis in this environment and therefore reliable estimates of atmospheric humidity are needed. In addition, hourly estimates of this variable are needed to evaluate the remotely sensed estimates of atmospheric water vapor. There are two alternative approaches that may be taken to account for this instrument failure. First, a daily estimate of atmospheric water vapor concentrations can be derived from the observed minimum daily air temperature (Running et al. 1987) under the assumption that this temperature is determined by the saturation vapor pressure and the relative humidity is therefore 100% at this temperature. This approach appears to produce reasonable approximations at a daily time step even though the hourly estimates are often in error.

In the satellite data analysis we needed accurate hourly estimates of atmospheric water vapor concentrations for comparison with the satellite water vapor estimates. We therefore attempted to estimate the effect of sensor degradation on the reported relative humidity measurements. We assumed that sensor response to 0% relative humidity was unchanged, but that loss of sensor material had decreased the sensitivity or "gain" of the instrument to atmospheric moisture. This sensor gain change could be determined by examining the evening measurements when saturation and therefore 100% relative humidity (RH) is typically observed. The sensor "gain" change was therefore approximated from departure between 100% RH and the observed "saturated" evening relative humidity. This gain adjustment approach produces a diurnal pattern of relative humidity measurements that differs from the minimum temperature approach. For example, the minimum temperature approach produces only one hour of 100% relative humidity per day, when the temperature is the lowest. The gain adjustment approach may produce several hours of 100% relative humidity, as long as the sensor is "saturated." This adjustment to the sensor record was carried out on a daily time step.

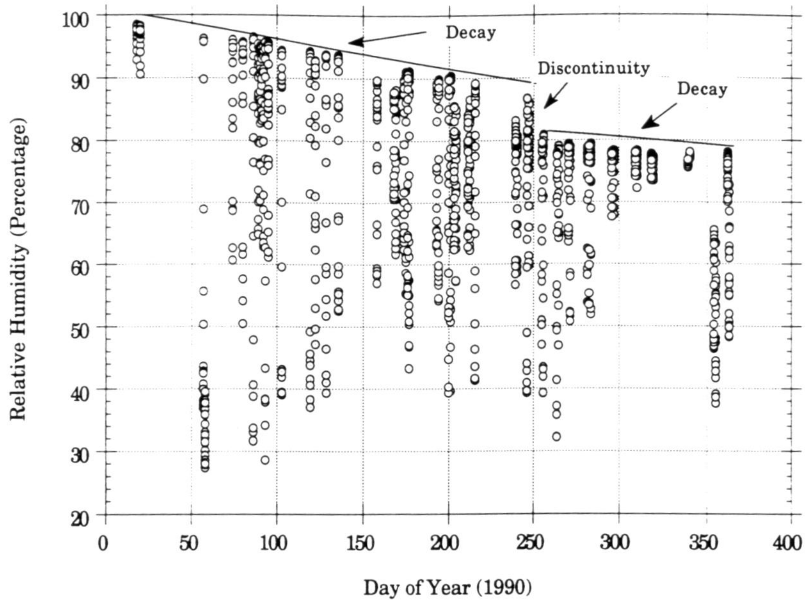

FIG. A1. Example of observed sensor degradation at site 1 in 1990. Each point represents an hourly observation. Satellite observation days are shown (⊙). The discontinuity appears to have occurred when the station was disturbed by a visit. Apparently more of the detector material was displaced from the sensor during visits. Similar patterns of decay were observed at all of the observatories.

We have no way of knowing whether this "gain" adjustment is a realistic description of the sensor performance degradation. Assessment of this approach would require comparison of a stable and a degrading sensor. However, given the need for accurate hourly relative humidity estimates, we saw no alternative to this attempt to reconstruct the un-degraded sensor record. We do believe that, for the purposes of this analysis, this approach is better than the minimum temperature reconstruction. Much of the residual error in the atmospheric humidity analysis may originate from the failure of these instruments and inability of this approach to reconstruct an uncorrupted record of the relative humidity conditions at the OTTER meteorological stations.